THE JOURNAL OF PHYSICAL CHEMISTRY C

Article

pubs.acs.org/JPCC

Understanding Local Bonding Structures of Ni-Doped Chromium Nitride Coatings through Synchrotron Radiation NEXAFS Spectroscopy

M. Mahbubur Rahman,[†] Zhong-Tao Jiang,*[,†] Zonghan Xie,[‡,△] Xiaofei Duan,[§] Zhi-feng Zhou,[∥] Pui Ching Wo,[⊥] Chun-Yang Yin,[#] Nicholas Mondinos,[†] Qinfen Gu,[&] Hantarto Widjaja,[†] Kevin Jack,[@] Anya Yago,[@] and Amun Amri[$]

[†]Surface Analysis and Materials Engineering Research Group, School of Engineering and Information Technology, Murdoch University, Murdoch, Western Australia 6150, Australia

[‡]School of Mechanical Engineering, University of Adelaide, Adelaide, SA 5005, Australia

[§]School of Chemistry, The University of Melbourne, Parkville, VIC 3010, Australia

[∥]Department of Mechanical and Biomedical Engineering, City University of Hong Kong, Kowloon Hong Kong, China

[⊥]School of Mechanical and Materials Engineering, Washington State University, Pullman, Washington 99164, United States

[#]School of Science and Engineering, Teesside University, Borough Road, Middlesbrough TS1 3BA, United Kingdom

[&]Australian Synchrotron, 800 Blackburn Rd., Clayton, VIC 3168, Australia

[@]Centre for Microscopy and Microanalysis, The University of Queensland, St. Lucia, QLD 4072, Australia

[$]Department of Chemical Engineering, Riau University, Pekanbaru, Indonesia

[△]School of Engineering, Edith Cowan University, Joondalup, WA 6027, Australia

ABSTRACT: CrN has widespread applications as protective coatings, for example, in aircraft jet engines whereby their high hardness and good oxidation resistance render metal components resistant to harsh operating conditions. Alloying elements are commonly incorporated (doped) into the coatings to further enhance their thermomechanical properties. However, the effect of dopants on the electronic properties and their roles in modifying the grain boundary configurations remain unclear. Lack of such critical knowledge has hindered the development of design strategies for high performance CrN-based coatings. To address this challenging issue, in the present study near-edge X-ray absorption fine structure (NEXAFS) investigations of $Cr_{1-y}Ni_yN$ coatings at the Cr $L_{3,2}$-edge (570−610 eV), Ni $L_{3,2}$-edge (840−890 eV), and N K-edge (380−450 eV) regions were conducted using synchrotron radiation soft X-ray (SXR) spectroscopy in both Auger electron yield (AEY) and total fluorescence yield (TFY) modes. The chemical states in CrNiN were found to change with the increase of Ni content, manifested as a small chemical shift and moderate change of shapes of various absorption edges. The CrN grain size also became smaller with increasing Ni concentration. These findings help improve our understanding of local bonding structures, which could potentially lead to improved coating designs for highly demanding applications.

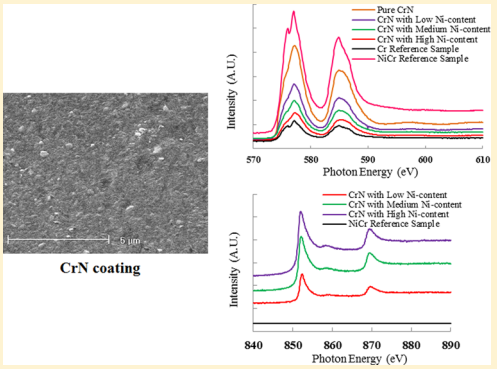

INTRODUCTION

Interests in transition metal nitrides have risen in the past few years due to their unique physical and mechanical properties that render them suitable for a wide range of technological applications in numerous devices.[1−13] For their superior strength, high corrosion, and oxidation resistance, these materials have been used in extreme pressure and temperature conditions, e.g., jet engine components. Moreover, dopants have been used to enhance their various physicochemical and mechanical properties such as hardness, oxidation resistance, inertness, diffusion resistance, and reflectance by the formation of dislocations, disorderness, vacancy, and atom substitution.[1,3−5,9] In addition, incorporation of Si, Al, or Ti into the CrN matrix results in the reduction of grain sizes down to the nanoscale, which enhances the hardness of the thin films.[2] At the nanoscale, the formation of dislocations becomes difficult, and the hardness of the thin coatings is thereby controlled by the grain boundary.[14]

Synchrotron radiation is emitted by very high-energy electrons circulating around a storage ring by a series of magnets separated by straight sections inside the synchrotron tunnels. Owing to their large skin depth in materials,

Received: May 21, 2014
Revised: July 23, 2014
Published: July 23, 2014

   dx.doi.org/10.1021/jp505004p | J. Phys. Chem. C 2014, 118, 18573−18579

synchrotron radiation can be directly used to probe the bulk and surface properties of the electronic structure of various material systems. X-ray absorption fine structure (EXAFS) spectroscopy, X-ray absorption near-edge structure (XANES), and near-edge X-ray absorption fine structure (NEXAFS) are powerful spectroscopic tools to enhance understanding of electronic structure and bonding states of the surface and interface of composite materials. The XANES technique is mainly used for the structural investigations of solids and inorganic complexes while NEXAFS is employed for characterization of materials surfaces.

Endrino et al.[1] studied the binary (TiN) and ternary (AlCrN) metal nitride coatings with silicon doping using X-ray diffraction (XRD) and NEXAFS techniques and found that they exhibited favorable physical hardness, toughness, and good oxidation resistance. The bonding structural evolution and the spectral changes were correlated in the X-ray absorption near-edge structure (XANES) studies of the aluminum incorporated titanium nitride[15] which afforded a comprehensive treatment on the local atomic structure of TiN. More recently, we[16] presented the bonding structural evolution in CrN coatings upon the progressive incorporation of Al and Si using NEXAFS spectroscopy in order to understand the change in electronic structure as the concentration of dopant varies. Evolution of the bonding structure was identified from shifts in the peaks of Al K-, Cr L-, and Si K-edge absorption energies. Further, the addition of Al and Si was found to play significant roles in tailoring the structure of the grain boundary within CrN coatings as well as the surface chemistry of the oxide layer, allowing the development of highly oxidation and corrosion resistant superhard coatings. In a comprehensive review, Chen[17] presented the NEXAFS investigations of transition metal nitrides, carbides, sulfides, and oxides along with other interstitial materials. Meanwhile, there are many attempts at producing new doping materials and improving their novel properties based on findings from the NEXAFS spectroscopy.[1,15,16,18−22] It is clearly evident that modifications of electronic and surface structures of transition metal nitrides remain a focus of research concerning thin film coatings in recent years. It should be noted that, however, the effects of Ni, Al, and Si doping elements on the electronic properties and surface structural evolution and their subsequent roles in modifying the grain boundaries of chromium nitride thin film coatings remain unclear. These effects could be revealed by utilizing the capabilities of a surface sensitive spectroscopic analytical technique. To further shed light on the electronic and surface properties of the doped Cr-nitrides, we performed NEXAFS measurements in surface-sensitive Auger electron yield (AEY) and bulk-sensitive total fluorescence yield (TFY) modes to discern the differences between the surface and bulk compositions of Cr nitrides with the dopants. Our present study is aimed at utilization of synchrotron radiation NEXAFS as a fingerprint technique to explore the local atomic structure of CrN coatings around Ni and investigate their changes with respect to the progressive doping of Ni^{2+} ions. The NEXAFS measurements have been carried out around Cr L-, Ni L-, and N K-edge for $Cr_{1-y}Ni_yN$ coatings.

EXPERIMENTAL SECTION

Deposition of $Cr_{1-y}Ni_yN$ Thin Film Coatings. $Cr_{1-y}Ni_yN$ (with y varied from 10 up to 40 at. %) thin film coatings with ∼2 μm thickness have been deposited on AISI M2 tool steel substrates using a TEER UDP 650/4 closed field unbalanced magnetron sputtering technique.[16] A four-target configuration manufactured by Teer Coatings Ltd., Droitwich, Worcestershire, UK, installed at the City University of Hong Kong has been used for this purpose. CrN coatings with low, medium, and high amount of Ni contents and three reference samples of CrN, NiCr, and Ni have been also prepared. All samples were mechanically cleaned in an ultrahigh vacuum by means of a diamond needle file and tungsten-wire brush for the NEXAFS study.

XRD Analysis. The structural information and phase identification of the $Cr_{1-y}Ni_yN$ thin film coatings were analyzed using X-ray diffraction (XRD). These analyses were conducted via Bruker Advance D8 X-ray diffractometer equipped with a LynxEye detector using Cu Kα radiation (λ = 1.5406 Å), operated at 40 kV and 40 mA at room temperature. The XRD scans of the $Cr_{1-y}Ni_yN$ thin film coatings were recorded in the angular range $10^\circ \leq 2\theta \leq 60^\circ$ in steps of 0.01°.

Synchrotron Radiation and NEXAFS Analysis of the Coatings. $Cr_{1-y}Ni_yN$ coatings were characterized by NEXAFS technique using the soft X-ray spectroscopy (SXR) beamline at the Australian Synchrotron facility in Melbourne. The storage ring was operated in the top-up mode with a beam current of 200 ± 1 mA at 3 GeV. A plane diffraction grating monochromator SX700 with a grating of 1200 lines/mm was used for collimating and monochromatizing the X-ray beam. For NEXAFS measurements, the samples were mounted on a stainless steel sample holder using double-sided carbon tapes to compensate for charging, and a minimum base pressure of 1×10^{-10} mbar has been maintained in the analysis chamber throughout. The photon energy used was 1253.6 eV. Measurements were conducted at a glancing incidence of 55°, the so-called "magic angle" with the X-ray beam. At the magic angle, possible effects of the preferred molecular orientations can be minimized for samples without azimuthal order. Two types of modes—Auger electron yield (AEY) and total fluorescence yield (TFY)—were used for the NEXAFS data record. For $Cr_{1-y}Ni_yN$ thin film coatings, NEXAFS data were recorded at Cr L-edge (570−610 eV), Ni L-edge (840−890 eV), and N K-edge (380−450 eV) in both modes with a channeltron facing the sample positioned 30° above the incoming beam and by monitoring drain current. The NEXAFS data recorded in AEY and TFY modes were normalized with respect to the incident photon flux by dividing the samples signal I_s with the incident photon flux I_0 monitored using a gold grid with high transmissivity positioned in front of the sample. The linear background was subtracted from the spectra by fitting the pre-edge region. The data were processed using SPECSLAB (V2.75-R25274) software.

RESULTS AND DISCUSSION

Structural Characterization of $Cr_{1-y}Ni_yN$ Thin Film Coatings. Figure 1 exhibits the XRD patterns of CrN and $Cr_{1-y}Ni_yN$ thin film coatings deposited by the magnetron sputtered technique. In Figure 1, CrN (111) and (200) can be identified at about 37.2° (peak B) and 43.2° (peak A) 2θ, respectively, based on (JCPDS 77-0047; space group 225). The (200) becomes broader, as well as decreases in intensity, as the Ni concentration is increased indicating the grain size crystallites of the CrN phase become smaller. This is consistent with the previous observation by Wo et al.[23]

Peak C at round 44.7° 2θ is due to (1) the iron-based substrate (JCPDS 87-0721; space group 229; (110)), (2) Ni_3N crystalline (JCPDS 89-5144; space group 182; (111)), and (3)

dx.doi.org/10.1021/jp505004p | J. Phys. Chem. C 2014, 118, 18573−18579

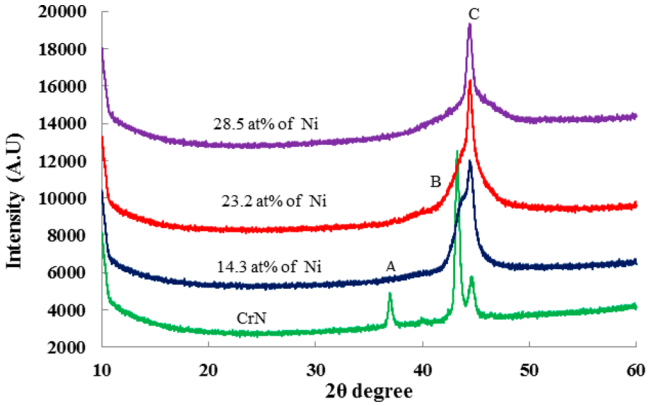

Figure 1. XRD pattern of Cr_{1-y} Ni_yN thin film coatings, where Ni varies from about 15 to 29 at. %.

metallic Ni (JCPDS 88-2326; space group 225; (111)). The iron (110) is seen in all the coating samples. The intensity of the peak at this position increases with addition of Ni atoms, indicating the appearance of the new Ni_3N and metallic Ni phases in the CrN matrix. The existence of Ni−N and metallic Ni bonds have been confirmed via XPS and reported in ref 23. The XPS results clearly showed elemental Ni bonding state dominating Ni−N bonding state (approximately 80%:20%). The broadening of base of the peak at 44.7° toward high 2θ may indicate the wide NixN composition distribution in the sample. The NEXAFS study below will give further discussion of the possible bonding states existing in the coatings.

Evolution of Cr and N in the Nickel-Doped $Cr_{1-y}Ni_yN$ Thin Films. Typically, X-ray absorption and/or emission spectroscopy probes the unoccupied and occupied densities of states of any compound on an element and orbital angular momentum based dipole selection rules. Generally, the NEXAFS of transition metal compounds are very sensitive to local ligand symmetry and d-shell electron occupancy. Because of the localized nature of p → d transitions for first-row transition elements, the multiplet phenomenological theory can be successfully applied for the interpretation of $L_{3,2}$-edge spectra of Cr and other transition elements.[24] The absorption around $L_{3,2}$-edges in transition metals originates from the transition of electrons from the 2p state to empty 3d states above the Fermi level. The two principal peaks with sharp intensities, the so-called white lines observed in the NEXAFS spectra (see Figures 2 and 3), correspond to the two transitions: $2p_{3/2} \rightarrow s_{1/2}, d_{3/2}, d_{5/2}$ (L_3) and $2p_{1/2} \rightarrow s_{1/2}, d_{3/2}$

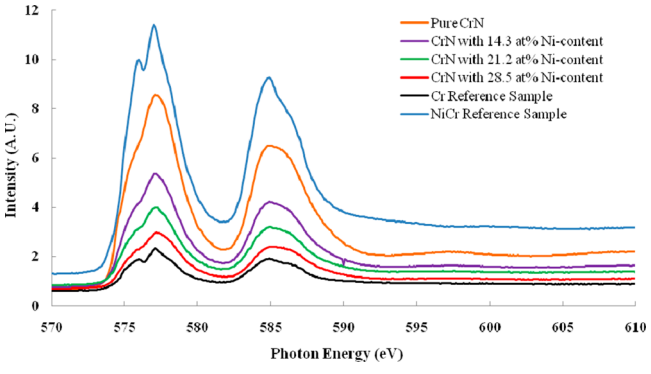

Figure 2. NEXAFS spectra of CrN, $Cr_{1-y}Ni_yN$, Cr reference, and NiCr reference coatings at Cr L-edge in AEY mode.

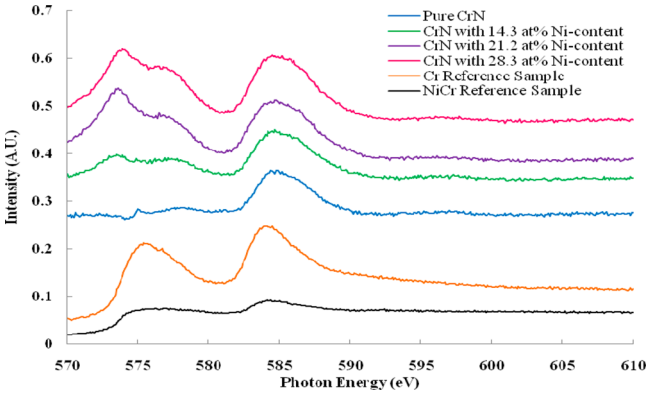

Figure 3. NEXAFS spectra of CrN, $Cr_{1-y}Ni_yN$, Cr reference, and NiCr reference coatings at Cr L-edge in TFY mode.

(L_2), respectively. The Cr $L_{3,2}$-edges originated from the spin−orbit coupling of the initial states and separated by an energy of ∼9 eV. In addition to the atomic and molecular electronic structures, the quantification of intensities of $L_{3,2}$-edges also provides information about the momentum, spin, and valence state.

Figures 2 and 3 show the Cr L-edge NEXAFS spectra of $Cr_yNi_{1-y}N$ thin films in pure state and doped with varying nickel content in the AEY and TFY mode. The NEXAFS spectra show that the local environments of nickel are of similar type with the progressive doping of nickel to the pure chromium nitride sample. In both modes, the first and second peaks are found at photon energies around ∼576.5 and ∼585 eV, respectively. Their intensities do not show any significant variation with the progressive Ni-content to the pure chromium nitrides, which in turn reveal the invariant nature of the local environments of Ni in the coatings. Comparing the NEXAFS data of $Cr_{1-y}Ni_yN$ with that of the Cr and NiCr reference coatings, it can be clearly seen that the spectral line shapes are of the same trend for the two reference samples. All the peak and edge positions of the two reference samples are matched with that of $Cr_{1-y}Ni_yN$ thin film coatings without any changes with the variation of Ni content. Thus, the existence of Cr and formation of NiCr is evident with the addition of Ni content to the pure CrN matrix. Two main peaks around the Cr $L_{3,2}$-edges are observed at ∼576.5 and 585 eV in both AEY and TFY modes. The absorption of Cr L-edge in AEY mode is much stronger than that in TFY mode, which may be attributed to the fact that the decay of the fluorescence yield in Cr L shell is less than the corresponding Auger yield. In Auger mode, the features found around 577 and 584 eV are similar to that of Cr_2O_3.[25] A small peak observed at ∼575 eV originates due to the transformations of Cr 1s state to the antibonding state arising from hybridizing between the Cr 4s and the N 2s states. This happens for the partial mixing of the N 2p state. The first peak which is observed around 576.5 eV can be assigned to a transition from Cr 1s core state to 3d states which reveals that the local structures around Cr atoms are C_{3v} symmetry. The small intensity and relative energy level of the peak is due to the transitions from Cr 1s state to antibonding state originating from the hybridization between Cr 4s state and N 2s state (forbidden transition) with the partial mixing of N 2p state. The separation between the L_3 and L_2 components is about 8.5 eV with some additional fine features arising from the multiplet effects. This separation energy is comparable with the width of the valence band. Additional fine structures basically arise from

dx.doi.org/10.1021/jp505004p | J. Phys. Chem. C 2014, 118, 18573−18579

the addition of an extra electron to the $3d^3$ configuration.[25] The scattering of electrons at the Cr $L_{3,2}$-edge stimulates the 3d → 3d transformations originating from the ligand field separation of the Cr 3d states. Furthermore, the $L_{3,2}$-edges absorption spectra of transition metal nitrides with unfilled d-shells may be explained on the basis of multiplet calculations and crystal field transformations from $2p^6d^n$ to $2p^5d^{n+1}$ state for an appropriate site symmetry determined by ligands. On the basis of multiplet calculations formation of Cr ligand with oxygen and other transition metals in normal bonding environments, there was a previous study that showed the sensitivity of L-edge spectra to the oxidation state and local symmetry of the metal.[26] It is well-known that the experimental identification of the Cr 3d states is complex; however, the band structures suggest that the Cr 3d states are comprised most of the valence band, and at the bottom of the valence band there is strong hybridization with the O 2p states. In contrast to the AEY spectrum, Cr L_3- and L_2-edges spectrum is approximately equally intense in the TFY mode. This is attributed to the fact that the fluorescence yield of chromium strongly depends upon the incident photon energy. This feature has been predicted by de Groot and coresearchers.[27] It is interesting to note that the Cr L-edge spectrum in CrN shows a slight difference at the energy position compared to $Cr_yNi_{1-y}N$ with different Ni concentration. A chemical shift of 0.40 eV to a high energy position in CrN is observed which is due to the different binding energy of the coating with the doping content.

Figures 4 and 5 represent the N K-edge NEXAFS spectra of $Cr_{1-y}Ni_yN$ thin film coatings in AEY and TFY modes recorded

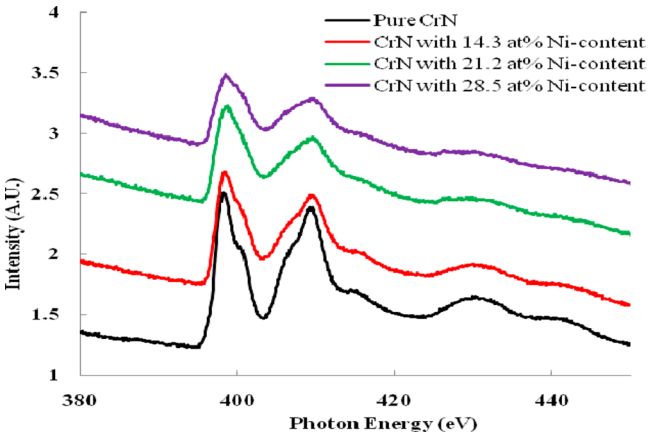

Figure 4. NEXAFS spectra of CrN and $Cr_{1-y}Ni_yN$ coatings at N K-edge in AEY mode.

in a vacuum analysis chamber. The same shape of the N K-edges spectrum in all samples indicate that the materials possess the same purity level, homogeneous structure, and zones with same type of elemental atomic ratios. Likewise, in the previous two cases, no obvious variations in the spectral line shape was detected with variation of Ni content to the CrN, suggesting that the local environment of Ni remains unchanged in CrN coatings. Both in AEY and TFY modes, the presence of the principal maxima and other peaks were almost at the same energy positions. The features seen at 398 and 401 eV are assigned to unoccupied N 2p states hybridized with Cr 3d orbitals, while the features around ∼409 eV to unoccupied N 2p states hybridizedwith Cr 4sp orbitals. The characteristic peak appearing at 398 eV is observed in all the NEXAFS spectra of our coatings which demonstrate that the Cr atoms are in the

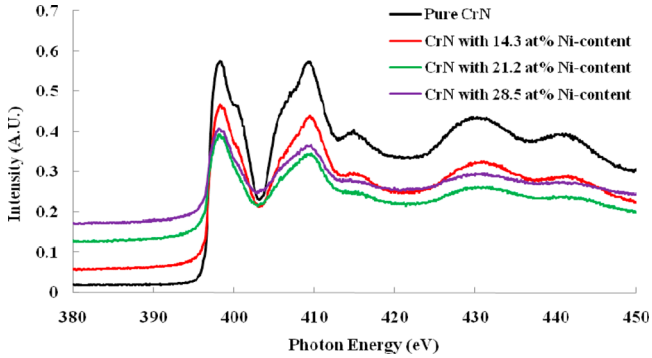

Figure 5. NEXAFS spectra of CrN and $Cr_{1-y}Ni_yN$ coatings at N K-edge in TFY mode.

center of a tetrahedron while the N atoms are at the corners. It was also observed that the intensity of the second main peak is lower than that of the first main peak in both modes. Our results show good consistency with previous report.[28] As the doping content is increased, a small shift in the second peak (from ∼0.5 to ∼1 eV) is noted along with the broadening of the N 2p feature. This could be related to the significant changes in spectral weight in the NEXAFS spectra of nitrogen 2p partial density of states observed around the valence band due to higher doping content. Similar features have been reported for GaN with Cr doping.[29] The modifications of intensity, observed with substantial addition of Ni, are associated with possible factors, such as variation in valence and alternation of the crystalline domains down to the nanoscale.

Significance of Dopant Ni in $Cr_{1-y}Ni_yN$ Thin Films. The $L_{3,2}$-absorption edges NEXAFS spectra of transition metal compounds provide information on the unoccupied orbitals associated with the oxidation state, spin state, and bond covalence. The Cr/Ni $L_{3,2}$-edge represents the dipole-allowed transition of a 2p electron into empty 3d and possibly 4s states (with $\Delta l = \pm 1$). The spin−orbit coupling results in a splitting of the metal L_3-edge ($2p_{3/2} \rightarrow 3d$) and L_2-edge ($2p_{1/2} \rightarrow 3d$). Figures 6 and 7 are NEXAFS spectra of the Ni $L_{3,2}$-edges for $Cr_{1-y}Ni_yN$ ternary compound with varying Ni contents as well as a NiCr reference sample for comparison. The intensities of the peaks have been found to be substantially enhanced with an increase in atomic percentages of Ni in the CrN coatings. However, no special features have been found on the NiCr reference sample at this absorption energy. This suggests that

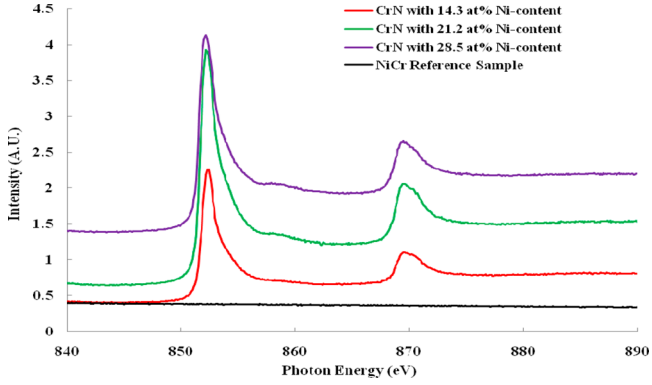

Figure 6. NEXAFS spectra of $Cr_{1-y}Ni_yN$ (with progressive addition of Ni content) and NiCr reference coatings at Ni L-edge in AEY mode.

dx.doi.org/10.1021/jp505004p | J. Phys. Chem. C 2014, 118, 18573−18579

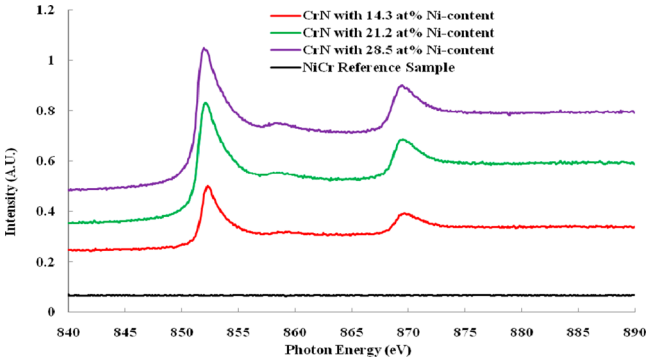

Figure 7. NEXAFS spectra of $Cr_{1-y}Ni_yN$ (with progressive addition of Ni content) and NiCr reference coatings at Ni L-edge in TFY mode.

there is no clear evidence of the formation of NiCr at the Ni L-edge of the $Cr_{1-y}Ni_yN$ coatings. The increase of the peak intensities of Ni L-edge spectrum, with increase of Ni, is associated with the increase in coordination and effective charge of Ni atoms. It is expected that, with an increase in Ni doping to the CrN matrix, the additional Ni will be located at octahedral positions in the phase. Since the absorption coefficient is proportional to the number of absorbing atoms and the absorption cross section, the intensity is eventually increased. In AEY and TFY modes, two main peaks are observed at positions ~852.2 and ~869.5 eV, respectively, along with a relatively marginal peak observed at ~858 eV. The peak positions and profiles of the spectra at ~852.2 and ~858 eV are similar to those of NiO_2.[30] In general, the L_3-edge absorption of NEXAFS spectra is sharper and more prominent because of the longer lifetime of the excited state.

The line shape and intensity of a spectrum are affected by the metal coordination environment and the number of conduction states. The intensity of the Ni $L_{3,2}$-edge absorption gradually increases with the progressive addition of Ni due to the presence of a large number of Ni-based conduction states and higher positively charged Ni atoms, e.g., Ni^{2+}. The Ni L-edges absorption in all the coatings is found to be at the same photon energy. This suggests that the binding energy of the Ni 2p level is the same in all the coatings and the electron density of empty Ni d-states is the same as the Fermi level in all the samples. The near-edge absorption structure of $L_{3,2}$-edge for 3d metals is governed mainly by that of the empty 3d states.[31,32] The intensity of the Ni $L_{2,3}$-edges for 3d metals depends on the number of the valence d-shell electrons, i.e., by the d-shell occupancy.[17] This indicates that the occupancy of the Ni d-shell in the $Cr_{1-y}Ni_yN$ becomes higher with increase in Ni content. In addition, higher electron transfer takes place with a marked difference in electronegativity between Cr and Ni. The symmetric Ni $L_{2,3}$-absorption edges of the NEXAFS spectra can be designated to the structure of the density of empty d-states of Ni, which does not change with the gradual increase of Ni content. This confirms the invariant nature of the Ni into the coatings. We also believe that with the increase in Ni, in the $Cr_{1-y}Ni_yN$ coatings, the direct bonds are formed by additional nickel Ni d-shell electrons. The generations of the direct d-bonds in the compound lead to the increase in resistance against crystal deformation, oxidation resistance, and wear resistance during the structural transformation. The NEXAFS measurements indicate that the absorption energy does not show any appreciable shift. In a previous study,[33] it was reported that the partial electron yield (PEY) and fluorescence electron yield (FEY) spectra were quite different from each other; however, in the present study the AEY and TFY spectra are found to be identical.

Implications of Electronic Configurations on Materials Properties of $Cr_{1-y}Ni_yN$ Coatings. The physicomechanical properties of nanocomposite coatings, consisting of nanocrystalline and/or amorphous phases, are a function of volume fractions of the mixing components and also influenced by the grain boundary configuration and size of the constituent phases. Owing to their very small grain sizes and abundant boundary zones surrounding individual grains, nanocomposite coating materials exhibit unique properties, e.g., superhardness and good toughness.[34] Superhardness of transition metal nitrides, e.g. CrN, have been achieved by adding various doping elements such as Si and Al.[9,35] The doping elements altered the microstructures of the binary compounds from closely packed columnar grains into nanocrystalline structures embedded in an amorphous matrix.[36] Doping by Al enhanced compressive stress, mechanical hardness, Young's modulus, resistance to elastic breakdown (H/E), and the plastic resistance (H^3/E^2) of CrN coatings with the highest amount of Al-content. Al atoms were found to be segregated around the grain boundaries to form an amorphous AlN structure.[35−37] The superhardness in CrN with Si and Al substitutions results from the combination of the fine-grain size together with the strong interfacial bonding between the nanocrystalline and amorphous phases.[9,35] Investigation of electrochemical behavior of CrN/Ni hard coatings on steel substrate established that the corrosion behavior of CrN coatings were significantly affected by the introduction of Ni as an interlayer.[38,39] The superior thermal stability of CrNiN and ZrNiN nanocomposite thin film coatings has also been reported by Karvánková et al.[40] In a recent study, Wo et al.[23] reported the microstructural and mechanical characterizations of CrN coatings with differing Ni contents. The gradual increase of Ni improved the damage tolerance and was found to be governed by intercolumnar shear sliding facilitated by high aspect ratio columnar grains.[23] The CrNiN coating system exhibited a good combination of high hardness and toughness with the increase of the Ni content.

High-resolution XPS spectra of the synthesized $Cr_{1-y}Ni_yN$, in the energy region of Cr 2p, were found to be decoupled into two stoichiometric peaks: referred to as CrN and Cr_2N. The occurrence of these two peaks shows a reduction of CrN phase and an increase of Cr_2N phase as Ni content was increased. This resulted in the reduction of hardness in the Ni containing coatings compared to the binary CrN system as shown in Figure 7 of ref 23. The addition of Ni content changed the deformation mechanism from grain boundary sliding in CrN to plastic deformation.[23]

The NEXAFS results from the $Cr_{1-y}Ni_yN$ coatings are able to explain the mechanical behavior of these coatings previously observed in a previous study.[23] The data in Figures 2−7 show no significant line shape changes, as Ni content is increased, in the near-edge spectra, suggesting that the angular character of the existing bonding is not affected by the addition of Ni. Although chemical states in the coatings changes with Ni introduction, less significant changes has been detected from the local environments of Ni, which means that the types of bonding existing in the coatings are the same in all coatings. It also appears that there are more direct d-bonds in Ni-containing CrN coatings. Recent nanoindentation study on the same set of $Cr_{1-y}Ni_yN$ coatings shows that although the hardness values of the coatings are maintained at a reasonably

dx.doi.org/10.1021/jp505004p | J. Phys. Chem. C 2014, 118, 18573−18579

high level (>15 GPa), a monotonic decrease in hardness occurred as Ni content increased from 15 to ~28 at. %.[23] This could be the result of an increase in d-suborbitals observed in the present study. In addition, an increase in peak intensities of Cr L-edge spectra was observed in high concentration of Ni, suggesting possible variations in valence, which could result in a reduction of crystalline domains, i.e., smaller grain size. This is a plausible explanation for the narrower (finer) grains observed in the $Cr_{1-y}Ni_yN$ from previous XTEM examinations.[23] The increase of the peak intensities of Ni L-edge spectrum, with increasing Ni concentration, indicates an increase in coordination and effective charge of Ni atoms with stronger bonds associated with the Ni atoms. This leads to stronger grain boundaries in the crystals. This agrees with the transition of deformation mechanism from grain boundary sliding in CrN to buckling of grains in $Cr_{1-y}Ni_yN$ as seen in a previous study.[23]

CONCLUSIONS

Comprehensive synchrotron radiation NEXAFS measurements were performed on Ni-doped CrN coatings to obtain a fundamental understanding of the influence of addition of Ni on the electronic and structural properties, in particular occupied and unoccupied Cr 3d, Ni 3d, and N 1s states, of $Cr_{1-y}Ni_yN$ coatings. It is shown that the chemical states in $Cr_{1-y}Ni_yN$ with different concentration of Ni are changing, as shown with the presence of a small chemical shift and moderate change of shapes of various absorption edges. This explains the reduction in grain size as Ni content increase in $Cr_{1-y}Ni_yN$ observed previously in a XTEM study and current XRD analysis. No significant changes in the NEXAFS spectral line shapes are detected with the progressive doping of Ni content to the CrN matrix, suggesting that the local environments of Ni remain unmodified in the samples. The higher peak intensities of Ni L-edge and Cr L-edge spectra obtained in CrN, with higher concentration of Ni, suggests an increase in valence, coordination number and effective charge of ions, and the existence of metallic Ni. The increase of Ni concentration reduces the hardness of $Cr_{1-y}Ni_yN$ coatings. However, the toughness of the coatings is enhanced, and the overall mechanical properties of the materials are improved possibly due to an increase in coordination and effective charge of the Ni atoms as observed in NEXAFS results. In the concentration range of Ni selected in this study, NEXAFS and previous studies did not show the optimal concentration for the highest hardness of the coatings. Further investigation with a wider range of Ni concentrations could provide a clearer explanation of the optimal condition for hardness and toughness for the overall mechanical properties of the coatings.

AUTHOR INFORMATION

Corresponding Author

*Tel +61 8 9360 2867; e-mail Z.Jiang@murdoch.edu.au (Z.-T.J.).

Notes

The authors declare no competing financial interest.

ACKNOWLEDGMENTS

M. Mahbubur Rahman is grateful to Murdoch University for providing financial support under the Murdoch International Postgraduate Scholarship (MIPS) program. Authors also acknowledge The University of Melbourne for providing the foundation access to the Australian Synchrotron. We also thank to Dr Anton Tadich of the Australian Synchrotron for his valuable discussion for the beamtime application. We also acknowledge the Australian Synchrotron for its travel support.

REFERENCES

(1) Endrino, J. L.; Palacín, S.; Aguirre, M. H.; Gutiérrez, A.; Schäfers, F. Determination of the local environment of silicon and the microstructure of quaternary CrAl(Si)N films. *Acta Mater.* **2007**, *55*, 2129−2135.

(2) Arnold, B. J.; Krishnamurthy, S.; Kennedy, B.; Cockburn, D.; McNally, D.; Lunney, J. G.; Gunning, R.; Venkatesan, M.; Alaria, J.; Michael, J.; et al. Growth and characterisation of Al1-xCrxN thin films by RF plasma assisted pulsed laser deposition. *e-J. Surf. Sci. Nanotechnol.* **2009**, *7*, 497−502.

(3) Kim, M. S.; Zhou, Y. K.; Funakoshi, M.; Emura, S.; Hasegawa, S.; Asahi, H. Tunnel magnetoresistance in GaCrN/AlN/GaCrN ferromagnetic semiconductor tunnel junctions. *Appl. Phys. Lett.* **2006**, *89*.

(4) Kimura, S.; Emura, S.; Tokuda, K.; Zhou, Y. K.; Hasegawa, S.; Asahi, H. Structural properties of AlCrN, GaCrN and InCrN. *J. Cryst. Growth* **2009**, *311*, 2046−2048.

(5) Zeng, F.; Chen, C.; Fan, B.; Yang, Y. C.; Yang, P. Y.; Luo, J. T.; Pan, F.; Yan, W. S. Effect of carbon doping on microstructure, electronic and magnetic properties of Cr:AlN films. *J. Alloys Compd.* **2011**, *509*, 440−446.

(6) Mycielski, A.; Kowalczyk, L.; Gałązka, R. R.; Sobolewski, R.; Wang, D.; Burger, A.; Sowińska, M.; Groza, M.; Siffert, P.; Szadkowski, A.; et al. Applications of II−VI semimagnetic semiconductors. *J. Alloys Compd.* **2006**, *423*, 163−168.

(7) Zeman, P.; Musil, J. Difference in high-temperature oxidation resistance of amorphous Zr−Si−N and W−Si−N films with a high Si content. *Appl. Surf. Sci.* **2006**, *252*, 8319−8325.

(8) Edgar, J. H. *Properties of Group III Nitrides*; INSPEC Institute of Electrical Engineers: Exeter, UK, 1994.

(9) Wo, P. C.; Munroe, P. R.; Li, Z.; Jiang, Z. T.; Xie, Z. H.; Zhou, Z. F.; Li, K. Y. Factors governing the mechanical behaviour of CrSiN coatings: Combined nanoindentation testing and transmission electron microscopy. *Mater. Sci. Eng., A* **2012**, *534*, 297−308.

(10) Petzow, G.; Herrmann, M. *Silicon Nitride Ceramics: Structure and Bonding*; Springer: Berlin, 2002; Vol. *102*.

(11) Pan, F.; Song, C.; Liu, X. J.; Yang, Y. C.; Zeng, F. Ferromagnetism and possible application in spintronics of transition-metal-doped ZnO films. *Mater. Sci. Eng., R* **2008**, *62*, 1−35.

(12) Yang, Y. C.; Pan, F.; Liu, Q.; Liu, M.; Zeng, F. Fully room-temperature-fabricated nonvolatile resistive memory for ultrafast and high-density memory application. *Nano Lett.* **2009**, *9*, 1636−1643.

(13) Orignac, X.; Barbier, D.; Du, X. M.; Almeida, R. M. Fabrication and characterization of sol-gel planar waveguides doped with rare-earth ions. *Appl. Phys. Lett.* **1996**, *69*, 895−897.

(14) Hirai, M.; Ueno, Y.; Suzuki, T.; Jiang, W.; Grigoriu, C.; K, Y. Characteristics of CrN films prepared by pulsed laser deposition. *Jpn. J. Appl. Phys.* **2001**, *40*, 1052−1055.

(15) Gago, R.; Redondo-Cubero, A.; Endrino, J. L.; Jiménez, I.; Shevchenko, N. Aluminum incorporation in $Ti_{1-x}Al_xN$ films studied by X-ray absorption near-edge structure. *J. Appl. Phys.* **2009**, *105*, 113521.

(16) Mahbubur Rahman, M.; Duan, A.; Jiang, Z.-T.; Xie, Z.; Wu, A.; Amri, A.; Cowie, B.; Yin, C.-Y. Near-edge X-ray absorption fine structure studies of $Cr_{1-x}M_xN$ coatings. *J. Alloys Compd.* **2013**, *578*, 362−368.

(17) Chen, J. G. NEXAFS investigations of transition metal oxides, nitrides, carbides, sulfides and other interstitial compounds. *Surf. Sci. Rep.* **1997**, *30*, 1−152.

(18) Tatsumi, K.; Mizoguchi, T.; Yoshioka, S.; Yamamoto, T.; Suga, T.; Sekine, T.; Tanaka, I. Distribution of solute atoms in β- and spinel $Si_{6-z}Al_zO_zN_{8-z}$ by Al K-edge X-ray absorption near-edge structure. *Phys. Rev. B* **2005**, *71*, 033202.

(19) Tanaka, I.; Nasu, S.; Adachi, H.; Miyamoto, Y.; Niihara, K. Electronic structure behind the mechanical properties of β-sialons. *Acta Metall. Mater.* **1992**, *40*, 1995−2001.
(20) Nouveau, C.; Djouadi, M. A.; Lambertin, M.; Da Silva, D. Influence of deposition conditions on the mechanical and structural properties of magnetron sputtered chromium nitride coatings. *Ann. Chim.: Sci. Mater.* **2003**, *28*, S137−S145.
(21) Endrino, J.; Palacín, S.; Gutiérrez, A.; Schäffers, F.; Krzanowski, J. Low and increased solubility of silicon in metal nitrides: evidence by X-ray absorption near edge structure. *J. Mater. Sci.* **2007**, *42*, 7607−7610.
(22) Gago, R.; Soldera, F.; Hübner, R.; Lehmann, J.; Munnik, F.; Vázquez, L.; Redondo-Cubero, A.; Endrino, J. L. X-ray absorption near-edge structure of hexagonal ternary phases in sputter-deposited TiAlN films. *J. Alloys Compd.* **2013**, *561*, 87−94.
(23) Wo, P. C.; Munroe, P. R.; Jiang, Z.-T.; Zhou, Z.; Li, K. Y.; Xie, Z. Enhancing toughness of CrN coatings by Ni addition for safety-critical applications. *Mater. Sci. Eng., A* **2014**, *596*, 264−274.
(24) De Groot, F. M. F. X-ray absorption and dichroism of transition metals and their compounds. *J. Electron Spectrosc. Relat. Phenom.* **1994**, *67*, 529−622.
(25) Arnold, T.; Payne, D. J.; Bourlange, A.; Hu, J. P.; Egdell, R. G.; Piper, L. F. J.; Colakerol, L.; De Masi, A.; Glans, P. A.; Learmonth, T.; et al. X-ray spectroscopic study of the electronic structure of $CuCrO_2$. *Phys. Rev. B* **2009**, *79*, 075102.
(26) Theil, C.; Van Elp, J.; Folkmann, F. Ligand field parameters obtained from and chemical shifts observed at the Cr $L_{2,3}$ edges. *Phys. Rev. B* **1999**, *59*, 7931−7936.
(27) de Groot, F. M. F.; Arrio, M. A.; Sainctavit, P.; Cartier, C.; Chen, C. T. Fluorescence yield detection: Why it does not measure the X-ray absorption cross section. *Solid State Commun.* **1994**, *92*, 991−995.
(28) Pflüger, J.; Fink, J.; Crecelius, G.; Bohnen, K. P.; Winter, H. Electronic structure of unoccupied states of TiC, TiN, and VN by electron-energy-loss-spectroscopy. *Solid State Commun.* **1982**, *44*, 489−492.
(29) Kim, J. J.; Makino, H.; Yamazaki, K.; Ino, A.; Namatame, H.; Taniguchi, M.; Hanada, T.; Cho, M. W.; Yao, T. Electronic structure of $Ga_{1-x}Cr_xN$ investigated by photoemission spectroscopy. *Curr. Appl. Phys.* **2004**, *4*, 603−606.
(30) Koyama, Y.; Mizoguchi, T.; Ikeno, H.; Tanaka, I. Electronic structure of lithium nickel oxides by electron energy loss spectroscopy. *J. Phys. Chem. B* **2005**, *109*, 10749−10755.
(31) Stöhr, J. *NEXAFS Spectroscopy*, 1992.
(32) Hüfner, S. *Photoelectron Spectroscopy: Principles and Applications*, 3rd ed.; Springer: Berlin, 2003.
(33) Yoon, W. S.; Balasubramanian, M.; Chung, K. Y.; Yang, X. Q.; McBreen, J.; Grey, C. P.; Fischer, D. A. Investigation of the charge compensation mechanism on the electrochemically Li-ion deintercalated $Li_{1-x}Co_{1/3}Ni_{1/3}Mn_{1/3}O_2$ electrode system by combination of soft and hard X-ray absorption spectroscopy. *J. Am. Chem. Soc.* **2005**, *127*, 17479−17487.
(34) Xu, J.; Li, Z.; Xie, Z.-H.; Munroe, P. Uniting superhardness and damage-tolerance in a nanosandwich-structured Ti−B−N coating. *Scr. Mater.* **2014**, *74*, 88−91.
(35) Li, Z.; Munroe, P.; Jiang, Z.-t.; Zhao, X.; Xu, J.; Zhou, Z.-f.; Jiang, J.-q.; Fang, F.; Xie, Z.-h. Designing superhard, self-toughening CrAlN coatings through grain boundary engineering. *Acta Mater.* **2012**, *60*, 5735−5744.
(36) Patscheider, J.; Zehnder, T.; Diserens, M. Structure−performance relations in nanocomposite coatings. *Surf. Coat. Technol.* **2001**, *146−147*, 201−208.
(37) Leyland, A.; Matthews, A. Design criteria for wear-resistant nanostructured and glassy-metal coatings. *Surf. Coat. Technol.* **2004**, *177−178*, 317−324.
(38) Creus, J.; Idrissi, H.; Mazille, H.; Sanchette, F.; Jacquot, P. Improvement of the corrosion resistance of CrN coated steel by an interlayer. *Surf. Coat. Technol.* **1998**, *107*, 183−190.
(39) Grips, V. K. W.; Ezhil Selvi, V.; Barshilia, H. C.; Rajam, K. S. Effect of electroless nickel interlayer on the electrochemical behavior of single layer CrN, TiN, TiAlN coatings and nanolayered TiAlN/CrN multilayer coatings prepared by reactive dc magnetron sputtering. *Electrochim. Acta* **2006**, *51*, 3461−3468.
(40) Karvánková, P.; Männling, H. D.; Eggs, C.; Veprek, S. Thermal stability of ZrN−Ni and CrN−Ni superhard nanocomposite coatings. *Surf. Coat. Technol.* **2001**, *146−147*, 280−285.